HAL open science

Understanding the temporal behavior of crops using Sentinel-1 and Sentinel-2-like data for agricultural applications

Amanda Veloso, Stéphane Mermoz, Alexandre Bouvet, Thuy Le Toan, Milena Planells, Jean-François Dejoux, Eric Ceschia

To cite this version:

Amanda Veloso, Stéphane Mermoz, Alexandre Bouvet, Thuy Le Toan, Milena Planells, et al.. Understanding the temporal behavior of crops using Sentinel-1 and Sentinel-2-like data for agricultural applications. Remote Sensing of Environment, 2017, 199, pp.415 - 426. 10.1016/j.rse.2017.07.015 . hal-03272371

HAL Id: hal-03272371

https://hal.science/hal-03272371v1

Submitted on 28 Jun 2021

HAL is a multi-disciplinary open access archive for the deposit and dissemination of scientific research documents, whether they are published or not. The documents may come from teaching and research institutions in France or abroad, or from public or private research centers.

L'archive ouverte pluridisciplinaire **HAL**, est destinée au dépôt et à la diffusion de documents scientifiques de niveau recherche, publiés ou non, émanant des établissements d'enseignement et de recherche français ou étrangers, des laboratoires publics ou privés.

Understanding the temporal behavior of crops using Sentinel-1 and Sentinel-2-like data for agricultural applications

Amanda Veloso, Stéphane Mermoz, Alexandre Bouvet, Thuy Le Toan, Milena Planells, Jean-François Dejoux, Eric Ceschia

CESBIO, Université de Toulouse, CNES/CNRS/IRD/UPS, Toulouse, France
amandaveloso@gmail.com (corresponding author)

Abstract:

Crop monitoring information is essential for food security and to improve our understanding of the role of agriculture on climate change, among others. Remotely sensing optical and radar data can help to map crop types and to estimate biophysical parameters, especially with the availability of an unprecedented amount of free Sentinel data within the Copernicus programme. These datasets, whose continuity is guaranteed up to decades, offer a unique opportunity to monitor crops systematically every 5 to 10 days. Before developing operational monitoring methods, it is important to understand the temporal variations of the remote sensing signal of different crop types in a given region. In this study, we analyse the temporal trajectory of remote sensing data for a variety of winter and summer crops that are widely cultivated in the world (wheat, rapeseed, maize, soybean and sunflower). The test region is in southwest France, where Sentinel-1 data have been acquired since 2014. Because Sentinel-2 data were not available for this study, optical satellites similar to Sentinel-2 are used, mainly to derive NDVI, for a comparison between the temporal behaviors with radar data. The SAR backscatter and NDVI temporal profiles of fields with varied management practices and environmental conditions are interpreted physically. Key findings from this analysis, leading to possible applications of Sentinel-1 data, with or without the conjunction of Sentinel-2, are then described. This study points out the interest of SAR data and particularly the VH/VV ratio, which is poorly documented in previous studies.

Keywords: Crops, Remote sensing, Multi-temporal Sentinel-1 data, optical data.

1. Introduction

There is a general demand for achieving optimal and sufficient crop productivity, while taking into account socio-economic conditions and the environmental impacts that the agricultural systems may cause. Crop management must be attentive to climate variability and adapt its practices according to given conditions. In this context, it is essential to achieve a full understanding of the processes driving the current patterns of crops production and also the cropland carbon, water and energy dynamics needed in implementation of climate change mitigation strategies.

Remotely sensing data can help to monitor crop growth by providing precise and timely information on the phenological status and development of vegetation. They constitute a valuable tool for tackling those issues at different scales, from local to global extents, especially when combined with agro-hydrological models for studies related to crop yield (Duchemin et al., 2015, Baup et. al, 2015), carbon (Veloso et al., 2014, Revill et al., 2013) and water budget (Le Page et al., 2014, Ferrant et al., 2014).

Optical data are used to explore the links between the photosynthetic and optical properties of the plant leaves, via vegetation indices. The most used is the Normalized Difference Vegetation Index (NDVI). Optical satellite images have significantly contributed to provide a range of crop added-value products, for instance crop area extent estimates, crop type maps (Inglada et al., 2015) and estimates of different biophysical parameters at various crop phenological stages (Quarmby et al., 1993, Doraiswamy et al., 2004, Baret et al., 2007, Bontemps et al., 2015). These applications have been widely developed based on data from various satellites, e.g. Landsat, MODIS and SPOT, although optical sensors are affected by the presence of clouds. Regarding synthetic aperture radar (SAR) data, studies have been carried out at various frequencies and incidence angles for interpreting crop temporal trajectories, based on electromagnetic modeling (Chiu et al., 2000, Cookmartin et al., 2000, Picard et al., 2002) and/or experimental data (Bush 1976, Engdahl et al., 2001, Hajnsek et al., 2007, Baghdadi et al., 2009, McNairn et al., 2014). Crop type maps using SAR have also been produced, for example by Dobson et al. (1996), Skriver et al. (2011) or Deschamps et al. (2012). However, compared to optical data, the use of SAR data in agricultural applications has not been well developed, partly due to the complexity, diversity and availability of SAR data, and partly due to the difficulty of data interpretation.

Up to now, monitoring crop dynamics was hampered by the lack of availability of high temporal and spatial resolutions satellite time series. A new era started with the launch of the first Sentinel satellite developed by the European Space Agency, providing a large and unprecedented amount of free data for the operational needs of the Copernicus program. Sentinel-1A, the first SAR satellite,

launched in April 2014, has started to provide multi-temporal series of SAR imagery (C-band) at an outstanding time interval of 12 days. With Sentinel-1B, launched in April 2016, the data provision is expected for every 6 days. Sentinel-2A, the optical satellite, launched in June 2015, provides data at a time interval of 10 days. With Sentinel-2B, the time interval will be 5 days. Those dense time series are not yet available worldwide, but for Europe Sentinel-1A and Sentinel-2A are already in operation. The dense time series of Sentinels offer a unique opportunity to systematically monitor crops at a weekly repeat cycle (from 5 to 12 days, depending of the data type and the region in the world). In addition, the continuity of Sentinel data is guaranteed up to 2030 and the next generation of Sentinel is planned beyond 2030, allowing long-term environmental monitoring.

So far, few studies have been using dense time series SAR data for crop monitoring. Only recently, Sentinel-1 data have been used (Navarro et al., 2016, Inglada et al., 2016). In order to derive methods using dense time series SAR and optical data, there is a need to study their temporal behavior for a variety of crop types that are widely cultivated. The objective of this paper is to analyse and interpret time series of Sentinel-1 data, and to compare the temporal variation with NDVI derived from optical data. The experimental dataset contain 28 Sentinel-1 data in 2014 and 2015 over our study area in the South of France. A multi-image filter (Bruniquel and Lopes 1997, Quegan and Yu 2001) was applied to reduce the speckle effect while preserving the spatial resolution and the fine structure present in the image. This strategy takes advantage of the Sentinel-1 dense temporal series and is particularly suited for monitoring even small crops. Since Sentinel-2 data were not yet available, we use a set of 71 data from different optical satellites that we will refer to as Sentinel-2-like data. The paper focuses on the analysis of the temporal behavior of SAR backscatter coefficients and NDVI of the main crop types in the temperate world (wheat and barley, rapeseed, maize, soybean and sunflower) over fields with varied management practices (e.g. tillage, sowing) and environmental conditions (rainfall, temperature). The study is conducted over 256 crop fields in Southwest France, surrounding two Joint Experiments for Crop Assessment and Monitoring (JECAM) experimental sites (Auradé and Lamasquère) that belong to the Regional Observation System (OSR) in Southwestern France.

The paper is organized as follows. The following section provides information on the study area and the data and Section 3 presents the results. Finally, conclusions are given in Section 4.

2. Study area and Data

2.1. Study area

The study area shown in Figure 1 is located in southwest France next to Toulouse and covers an area of approximately 70 x 40 km. The study region is mainly covered by arable lands (approximately 60%). The main cultivated crops are wheat (*Triticum aestivum* L.), barley (*Hordeum vulgare* L.), rapeseed (*Brassica napus* L.), maize (*Zea mays* L.), soybean (*Glycine max* (L.) Merr.) and sunflower (*Helianthus annuus* L.). The climate in the region is temperate and mild and is characterized by warm and dry summers, sunny autumns, mild winters and rainy springs. The annual mean precipitation is approximately 656 mm, and the annual mean temperature is 13°C. The Garonne River crosses the study area, and the soil textures are mainly clay and loam. However, most of the maize and sunflower crops in this study are cultivated over silty (boulbenes) and clayey limestone soils respectively.

A set of 256 fields were surveyed on the ground at different dates for providing land-use data. The crop type classes included in the dataset and the amount of surveyed fields per class are: wheat (64), barley (1), sunflower (116), maize (57), rapeseed (10) and soybean (8). The surface area of the fields varies between 1.75 and 45 ha. Table 1 presents the typical calendar of some of the main phenological stages and management practices for the investigated crop type classes.

Table 1: Average periods of the main phenological stages for different crop types in the study area

		Sowing	Emergence	Heading/Flowering	Harvest
Winter crops	**Wheat & Barley**	Mid-October – late November	Sowing + 15 days	Late April – early May	Late June – mid-July
	Rapeseed	Late August – September	Sowing + 15-30 days	April	Late June – early-July
Summer crops	**Maize & Soybean**	Mid-April – late May	Mid-May – mid-June	July	1-15 September (silage) October (grain)
	Sunflower	Early April – mid-May	Sowing + 10 days	1-20 July	September

In the study area, two agricultural sites have been intensively monitored since 2005, the so-called Auradé (shown in Figure 2) and Lamasquère sites (Béziat et al., 2009). The two sites are part of the FLUXNET global network [http://fluxnet.ornl.gov] and the Joint Experiment for Crop Assessment and

Monitoring [JECAM: http://www.jecam.org/project-overview/france-osr] networks. They are also Integrated Carbon Observation System (ICOS) sites and therefore, meteorological and flux measurements are standardized according to the ICOS protocols. In addition, fresh biomass and ***green area index*** (GAI) have been measured in both sites in 2015. ***The concept of GAI (Baret et al., 2010, Duveiller et al., 2011) corresponds to the photosynthetically active plant area without organ distinctions. We preferred to use the GAI instead of LAI because it is better correlated with remote sensing observations.***

The two sites have similar climatic conditions but different soil properties, topography and management practices. It is noted that Auradé and Lamasquère crop rotations are representative of the main regional crop rotations.

The Auradé plot (23.5 ha) is located on a hillside area near the Garonne river terraces and is characterized by a rapeseed - winter wheat - sunflower - winter wheat four-year rotation that only receives mineral fertilizers and does not receive irrigation. Only the grain is exported whereas all other parts of the plants are left. Superficial tillage (5–10 cm depth) is usually done after harvest to plough residues, spontaneous regrowth and weeds into the soil. The Lamasquère plot (23.8 ha) is part of an experimental farm owned by the Purpan Engineering School EIP (Ecole d'Ingénieurs de Purpan) and is characterized by a maize - winter wheat two-year rotation that is used to feed livestock and provide litter. Therefore, nearly all aboveground biomass is exported as grain and straw for winter wheat, and maize is harvested when it is still green for silage. Both organic and mineral fertilizers are applied and the maize is irrigated. **In the 2015 season, a hose-reel irrigator was used. This field was irrigated 5 times between May and August.** Superficial tillage after harvest may be performed, depending on the cultivated crops. Deep tillage (30 cm depth) is usually performed in November before sowing of summer crops (essentially maize).

For the 2014-2015 agricultural season considered in this study, barley was cultivated (instead of wheat) at Auradé and maize at Lamasquère. Their crop growth and development will be investigated in detail in section 3.

2.2. Field data

2.2.1. Vegetation data

For the Auradé and Lamasquère plots, destructive measurements of **green area index (GAI)** and fresh and dry aboveground biomass were performed regularly to characterize crop development during the vegetative cycle (five times each site). **Measured GAI is defined as the half-surface of all green organs. It was measured by means of a LiCor planimeter (LICOR 3100, Lincoln Inc., Nebraska).** For maize in Lamasquère, twenty plants were collected at each date along a transect

crossing the plot. For barley in Auradé, ten 0.25 m long rows were collected at each sampling date. Plant height was also measured. Yield data were provided by the farmers who cultivate the two sites.

2.2.2. Meteorological data

Air temperature and precipitation measurements were continually recorded over the Auradé and Lamasquère sites (Béziat et al., 2009). Data were originally pre-processed and delivered at a time scale of 30 min. For this study, air temperature recorded at 6 a.m. was selected, which corresponds to the approximate time of the Sentinel-1 data acquisition. The precipitation measurements were integrated to obtain daily values. The Lamasquère site temperature values were used qualitatively in the analysis of the results for all the 256 other fields under study, assuming that temperatures do not change drastically within the study area. However, precipitation data over the 256 other fields were derived from the Global Satellite Mapping of Precipitations (GSMaP) project (Aonashi et al., 2009). The GSMaP project provides precipitation data based on the combined microwave-infrared algorithm using GPM-Core GMI, TRMM TMI, GCOM-W1 AMSR2, DMSP series SSMIS, NOAA series AMSU, MetOp series AMSU, and Geostationary infrared developed by the GSMaP project. The newly developed algorithm for the Global Precipitation Measurement (GPM) mission (GPM-GSMaP Ver.6) is used to retrieve rainfall at 0.1 degree latitude/longitude resolution every hour. We assigned for each crop the corresponding daily rainfall value.

2.2.3. Soil water content data

At Auradé and Lamasquère sites, theta probes ML2X (DeltaT devices) measuring volumetric soil water content (SWC) were settled in 3 independent pits, at 0.5 cm and 5 cm depth. A site-specific calibration function, determined with gravimetric measurement, was applied to convert the mV signal into volumetric SWC. **The root mean square error (RMSE) and the square of the Pearson's linear correlation coefficient (r^2) related to the linear regression between the mV signal and the SWC were 5.6% and 0.57 respectively over the Auradé site and 3.2% and 0.87 respectively at the Lamasquère site**. Then, volumetric SWC was estimated by averaging the 3 measurements. Data were delivered at a time scale of 30 min, and averaged at daily time step.

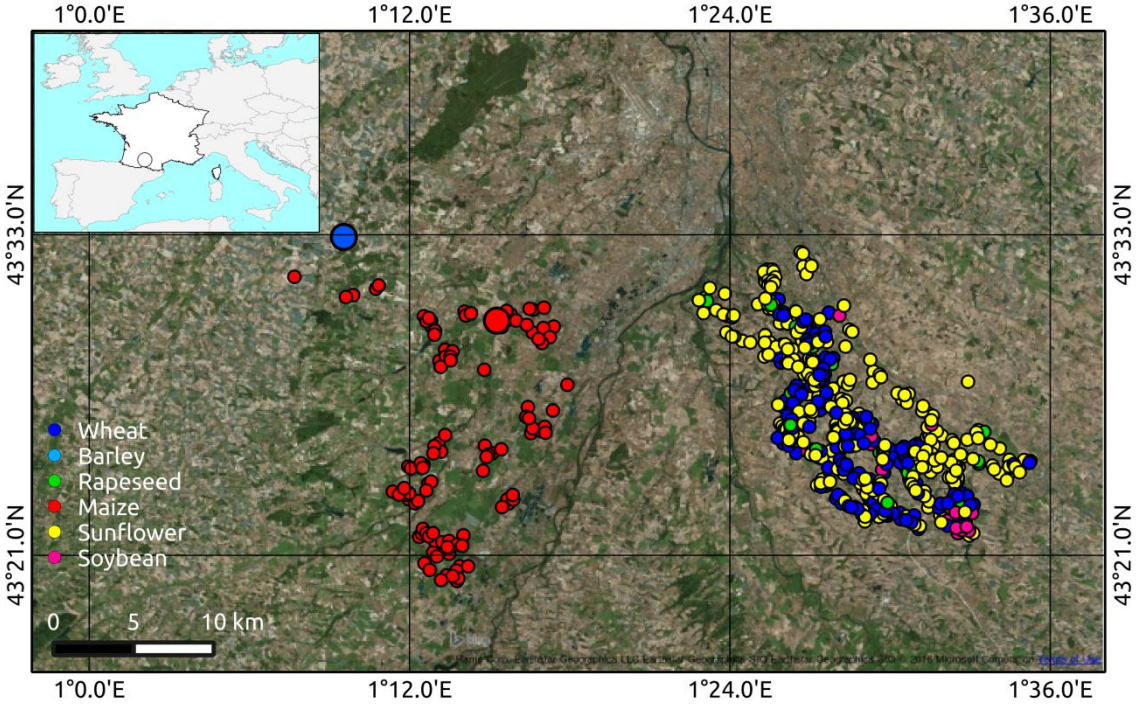

Figure 1: Field data over a 70x40 km area in South-West France, superposed to very high resolution optical data from Bing Map. Large circles represent the two Joint Experiment for Crop Assessment and Monitoring (JECAM) experimental sites (Auradé and Lamasquère). Small circles represent the other crop fields studied in this paper. In this area, in average between 2006 and 2013, 43% of cultivated crops were cereals, 25% were sunflower, 5% were maize and 5% rapeseed, (from detailed French national land use database, the RPG (in French, *Registre Parcellaire Graphique*).

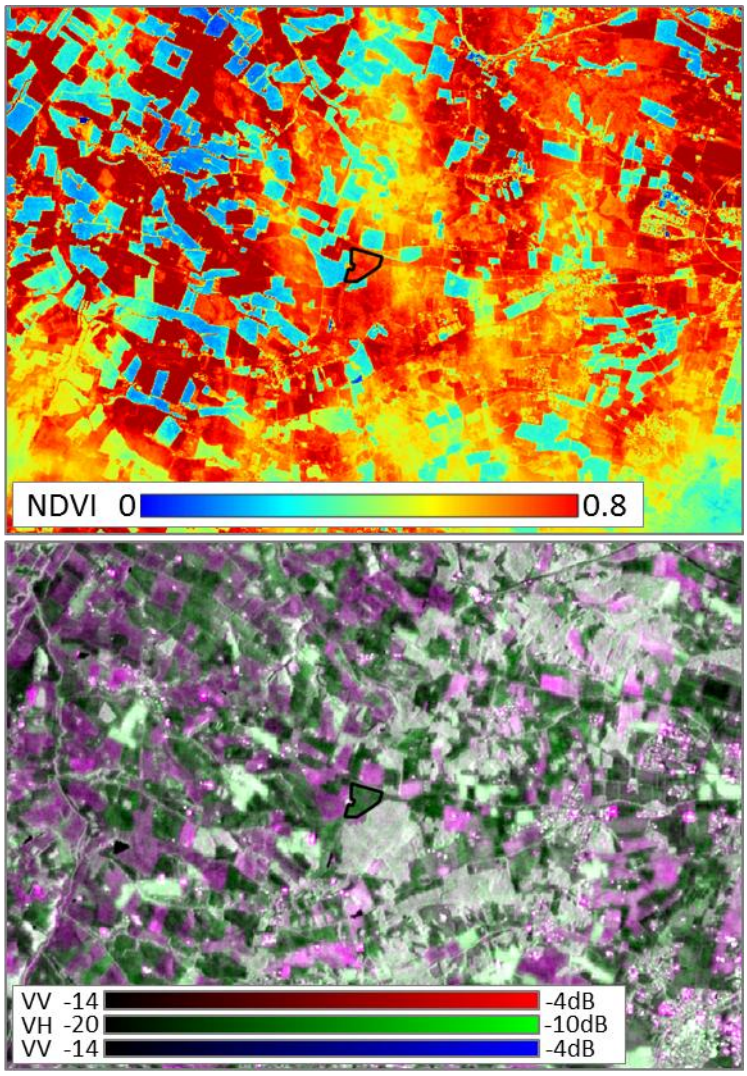

Figure 2: The experimental site of Auradé (surrounded in black) and its surroundings. Auradé is located 28 km south-west of Toulouse, in France. At the top, the NDVI map derived from a SPOT5-Take5 image (10 m resolution) acquired on 29 April 2015; at the bottom, an RGB image of VV and VH backscatters from a Sentinel-1 image (20 m resolution) acquired on 5 May 2015. Vegetated areas appear in green. The 17.5 x 12.5 km area is centered on 43.549°N, 1.106°E.

2.3. Remote Sensing data

2.3.1. SAR data

Twenty-eight Sentinel-1A images have been acquired between 6 November 2014 and 7 December 2015. The ESA Sentinel-1 observation strategy defines the Interferometric Wideswath (IW) mode as the pre-defined mode over land. This mode provides dual-polarisation (VV and VH) imagery, at a resolution of 10 meters, with a swath of 250km. The incidence angle over the surveyed fields shown in Figure 1 ranges approximately from 38 to 41°.

All the Sentinel-1 imagery is made available free of charge by ESA. In this study, we used Level-1 Ground Range Detected (GRD) products that consist of focused SAR that has been detected, multi-looked and projected to ground-range using an Earth ellipsoid model. The data have been first calibrated to obtain the γ^0 backscatter coefficient, **using the "Calibration" module in the Sentinel Application Platform SNAP (ESA, 2017)**.

We additionally multi-looked the data with a window size of 2x2 **("Multilooking" module in the SNAP)** to reduce the speckle noise effect, reaching a spatial resolution of 20m. Then, terrain correction was applied **("Range-Doppler Terrain Correction" module in the SNAP)** to geocode **accurately** the images by correcting SAR geometric distortions (foreshortening, layover and shadow) using the digital elevation model from the Shuttle Radar Topography Mission (**that allows to take into account the local elevation variations**). The images are therefore overlaid, without additional coregistration. A speckle filter (Bruniquel and Lopes 1997, Quegan and Yu 2001) was then applied to further reduce the speckle effect while preserving the 20m spatial resolution and the fine structure present in the image. As evidenced for example in Mermoz et al. (2014, 2016), this filter produces images with reduced speckle effects from multi-temporal (28 dates) and multi-polarised (VH and VV) images, and is expressed as follows:

$$J_k(\upsilon) = \frac{\langle I_k(\upsilon)\rangle}{N} \sum_{i=1}^{N} \frac{I_i(\upsilon)}{\langle I_i(\upsilon)\rangle} \quad \text{with } k=1,\ldots,N \qquad (1)$$

where $J_k(\upsilon)$ is the radar intensity of the output image k at pixel position υ, $I_i(\upsilon)$ is the radar intensity of the input image i, $\langle I_i(\upsilon)\rangle$ is the local average intensity of the input image ***i*** (window size of 7x7) and N is the number of images. **We implemented this filter using the Matlab software (R2011 version). The resulting theoretical equivalent number of looks (*ENL*) was estimated using the following equation (Quegan and Yu 2001):**

$$\boldsymbol{ENL = L\,\frac{M.N}{M+N-1}} \qquad (2)$$

where L is the initial number of looks, M the number of images (28 dates x 2 polarisations) using a fixed window size of N pixels (7x7 pixels). L is found to be 17,6 that is the product of approximately 4.4 initial looks for GRD data at 10m (ESA report, 2016) multiplied by 4 (multi-look of 2x2). According to equation 2, the final theoretical ENL per pixel is 464. In the following, the ENL per crop is even much higher as tens to hundreds of pixels were grouped to derive average values by crops.

Radar backscatter is affected by factors related to crop biomass, structure and ground conditions. Past studies agreed that the observed backscatter at C-band is a combination of the ground backscatter attenuated by the canopy layer and the backscatter from the canopy, which includes simple and multiple scattering, and the vegetation-ground interaction **(Attema and Ulaby, 1978; Ulaby et al., 1986; Bouman and Hoekman, 1993)**. The backscatter from vegetation canopy is affected by vegetation 3D structure and water content (related to biomass) **(Karam et al., 1992)**. The ground backscatter at C-band is affected by soil moisture, surface roughness and terrain topography **(Schmugge, 1983)**. Note that the moderate topography of the plots used in this study (mean slope of 4.3^{o}), together with the Sentinel-1 processing that reduced radiometric and geometric distortions, ensure low topographic effects. The vegetation-ground interaction depends on both vegetation and ground characteristics **(Brown et al., 2003)**. The relative importance of these 3 scattering components depends on the radar frequency, polarisation, incidence angle, the crop type and growth stage, and the ground conditions. In general, the ground scattering is dominant at the early and late crop growth stage, and in-between vegetation scattering dominates (Mattia et al., 2003). However, during the period when the vegetation scattering is more important, the relationship between the radar backscatter and the vegetation biophysical parameters is considerably influenced by the dynamics of the canopy structure, including orientation, size and density of the stems and the dielectric constant of the crop elements, which depend on the phenological stage. For example, a drastic difference in the sensitivity of backscatter to wheat biophysical parameters has been found before and after the heading stage by Mattia et al. (2003). In terms of incidence angle, the shallow incidence angles (>35-40°) increase the path length through vegetation and maximize the vegetation scattering contribution (Blaes et al., 2006), whereas steep incidence angles (<30°) reduces the vegetation attenuation and maximize the ground scattering contribution in the return, which is more useful for soil moisture measurement (Mattia et al., 2006). In our datasets, the incidence angles are approximately 40° (38° to 41°), the data are therefore suitable to the crop parameters retrieval. Regarding the polarisation effect, it is well known that HH is more sensitive to surface scattering and HV to volume scattering, and VV a combination of the two. HV backscatter is therefore often used for the retrieval of crop parameters, and HH, ground parameters. However, theoretical modeling and ground-based SAR measurements have indicated that VH and VV can contain vegetation ground interaction (double-bounce term) (Picard et al., 2003). **In fact, soil returns at VH polarisation is probably caused by double scattering (stem-ground) (Brown et al., 2003). This hypothesis is supported by simulation results based on a second-order radiative transfer model (Brown et al., 2000), showing that double-bounce scattering exceeds the direct backscatter from the soil**. In this case, the ratio VH/VV can reduce the double-bounce effect. **In addition, the ratio VH/VV probably reduce errors associated to the acquisition system (e.g. due to the radiometric stability) or**

environmental factors (e.g. due to variations of soil moisture) and might appear as a more stable indicator in time than VH or VV backscatter. Nevertheless, the scattering mechanisms are in general much more complex and experimental observations are needed to provide insights into the scattering behavior of each crop type.

For additional information on interactions between electromagnetic waves and crops, in particular using multipolarisation or polarimetric data at C-band, you may refer to the thorough review of McNairn et al. (2004). For a recent and complete review on the use of SAR data (including PolSAR, PolInSAR or TomoSAR techniques at various frequencies) or even scatterometers and radiometers for applications in agriculture, please read Steele-Dune et al. (2017).

2.3.2. Optical data

Seventy-one Sentinel-2-like optical images have been acquired by four satellites, SPOT5-Take5 (39 acquisitions), Landsat-8 (27 acquisitions), Deimos-1 (3 acquisitions) and Formosat-2 (2 acquisitions), between 2 November 2014 and 25 December 2015.

Formosat-2 is a Taiwanese satellite that provides images with spatial resolution of 8 m in four visible and near-infrared reflective bands. Images are taken at nearly constant viewing angles. Deimos-1 provides 22 m resolution images in three spectral bands (red, green and near-infrared) that have been designed to be compatible with the same channels of the Landsat series, allowing full compatibility. The Landsat 8 is an American satellite, launched in 2013, that provides multispectral images (at nine spectral bands) along the entire Earth at 30 m resolution with a repeat cycle of 16 days.

In the frame of the SPOT Take 5 experiments, the Centre National d'Etudes Spatiales (CNES) lowered the orbit altitude of SPOT, to place it on a five-day repeat cycle orbit for a given duration. Images were acquired at 10 m resolution every 5 days under constant angles, at four spectral bands (green, red, near infrared and short wave infrared). Data were processed by THEIA [www.theia-land.fr] Land Data Center and were distributed with a free and open policy for scientific purposes.

The four optical remote sensing datasets were pre-processed using the Multi-sensor Atmospheric Correction and Cloud Screening prototype (MACCS, Hagolle et al., 2008, 2015) spectro-temporal processor. One particularity of MACCS is that it uses multi-temporal criteria to build cloud, cloud shadow, water and snow masks and to detect the aerosols before the atmospheric correction. All datasets were processed to level 2A within the THEIA Land Data Center.

Next, NDVI was computed. Note that the NDVI time series were not smoothed despite the different spatial and spectral resolutions of the four optical sensors. However, we consider that these differences do not have a significant effect on the NDVI estimates as they were averaged over each field within surface areas ranging from 1.75 to 45 ha.

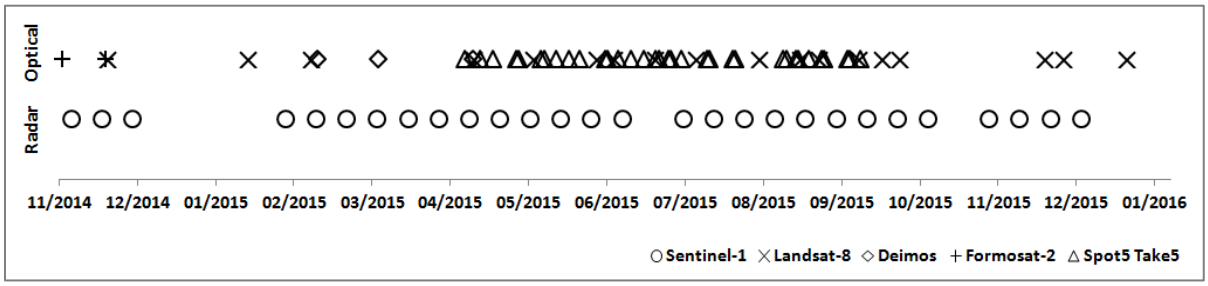

Figure 3: Calendar of the remote sensing data acquisitions, expressed in month/year. At the top, the 71 optical data acquisitions from: Landsat-8 (cross), Deimos (diamond), Formosat-2 (plus) and SPOT5-Take5 (triangles). At the bottom: 28 radar acquisitions from Sentinel-1 (circle).

3. Results and Discussion

The time series of optical NDVI and radar backscatter (VH, VV and VH/VV) are analysed and physically interpreted with the support of rainfall and temperature data, as well as the destructive in situ measurements (GAI and fresh biomass, when available). The analysis is performed for each crop type separately, grouped in winter and summer crops. The square of the Pearson's linear correlation coefficient r^2 indicated in this section represents correlation between temporal interpolated NDVI and SAR backscatter **(VV, VH and VH/VV). The number of available SAR observations during the growth cycle determines the number N of samples used for computing these correlations. The NDVI profiles were interpolated (using a third degree polynomial) to have corresponding NDVI values at the SAR acquisition dates.**

3.1. Winter crops

3.1.1. Cereals (Barley and Wheat)

Barley and wheat are two cereals that are grown as winter crops in the study area, with a very similar plant structure and phenology. They are therefore treated in the same subsection, first by analysing in detail one barley field with associated *in situ* data, and then a set of 64 wheat fields. **Note that the results and analysis below for barley, based on one single field, might be not fully representative of the barley crop behavior.**

Barley in the Auradé site was sown on 22 October 2014, emergence occurred approximately on 5 November 2014, and the field was harvested on 27 June 2015. The corresponding remote sensing time series are shown in Figure 4. The most striking feature is the sensitivity of the VH/VV ratio to the barley growth cycle. While NDVI starts increasing immediately after the emergence of barley plants and appears therefore correlated to the greenness of small vegetation, VH/VV remains relatively stable during winter and starts increasing significantly at the tillering stage, around beginning of March. In fact, VH/VV is always more correlated to the fresh biomass than to the photosynthetic activity.

VH/VV appears more stable in time than VH or VV backscatter as anticipated and detailed in section 2.3.1., and more sensitive to the barley growth cycle. But although the VH and VV profiles appear complex, most of their variations can be physically explained. During winter, the vegetation remains short and VV and VH are affected mostly by variations in the soil backscatter driven by SWC and surface roughness. For example, rainfall events just before the two first Sentinel-1 acquisitions may explain the slight increase of the backscatter. Then, a slight decrease of VV and VH backscatters is observed until beginning of March, which can be explained by the soil backscatter attenuated by the growing vegetation, plus probably by the progressive smoothing of the soil until early April 2015. Note that the strong and abrupt decrease of VV and VH backscatters on 10 February 2015 (observed in all the fields regardless the crop type) is caused by the frost (Khaldoune et al., 2009) as confirmed by the temperature records. At the tillering stage in March and during the stem elongation phase in April, the volume fraction of the vegetation increases as a result of the increase in the number of stems per plant and in the length of these stems. The VH backscatter, which is dominated by the attenuated double-bounce and volume scattering mechanisms, increases **as reported in Lopez-Sanchez et al. (2013) and Wiseman et al. (2014)**, while the VV backscatter, which is dominated by the direct contribution from the ground and the canopy, decreases due to the rising attenuation from the predominantly vertical structure of the barley stems (Brown et al., 2003), especially in April, during the stem elongation (Jia et al., 2013). Note that under drier meteorological conditions at the same period, the contribution of ground vegetation interaction in the VH backscatter may decrease compared with the volume contribution, leading to a more increasing VH backscatter.

The resulting VH/VV therefore increases until end of April, whereas NDVI remains stable from beginning of March. At the beginning of May, the observed increase in VH and VV is related to the heading (that causes an increase in the fresh biomass), as previous experimental (Mattia et al., 2003) and theoretical (Picard et al., 2003) studies have found for similar frequencies and incidence angles. This illustrates the potential of Sentinel-1 time series to capture very short phenological events. During the senescence, which starts at the beginning of June, both the NDVI and the VH/VV ratio are

characterized by a steady decrease until harvest, as a consequence of the decreasing chlorophyll and water content.

Another important finding is the capacity of VH/VV to detect post-harvest spontaneous regrowth (refer to the photographs in Figure S1), which is visible in the form of a second cycle (Figure 4) from end of July to beginning of October at the Auradé site. The regrowth is due to a combination of soil work on 20th July, which together with the rainfall events, allowed the grain fallen on the soil at harvest to emerge in the beginning of August (stale seedbed). This is a promising result for future applications such as the monitoring of post-harvest events, like regrowth and cover crops, which store carbon in agricultural soils (Poeplau and Don, 2015, Ceschia et al., 2010) and therefore represent interesting levers for climate change mitigation.

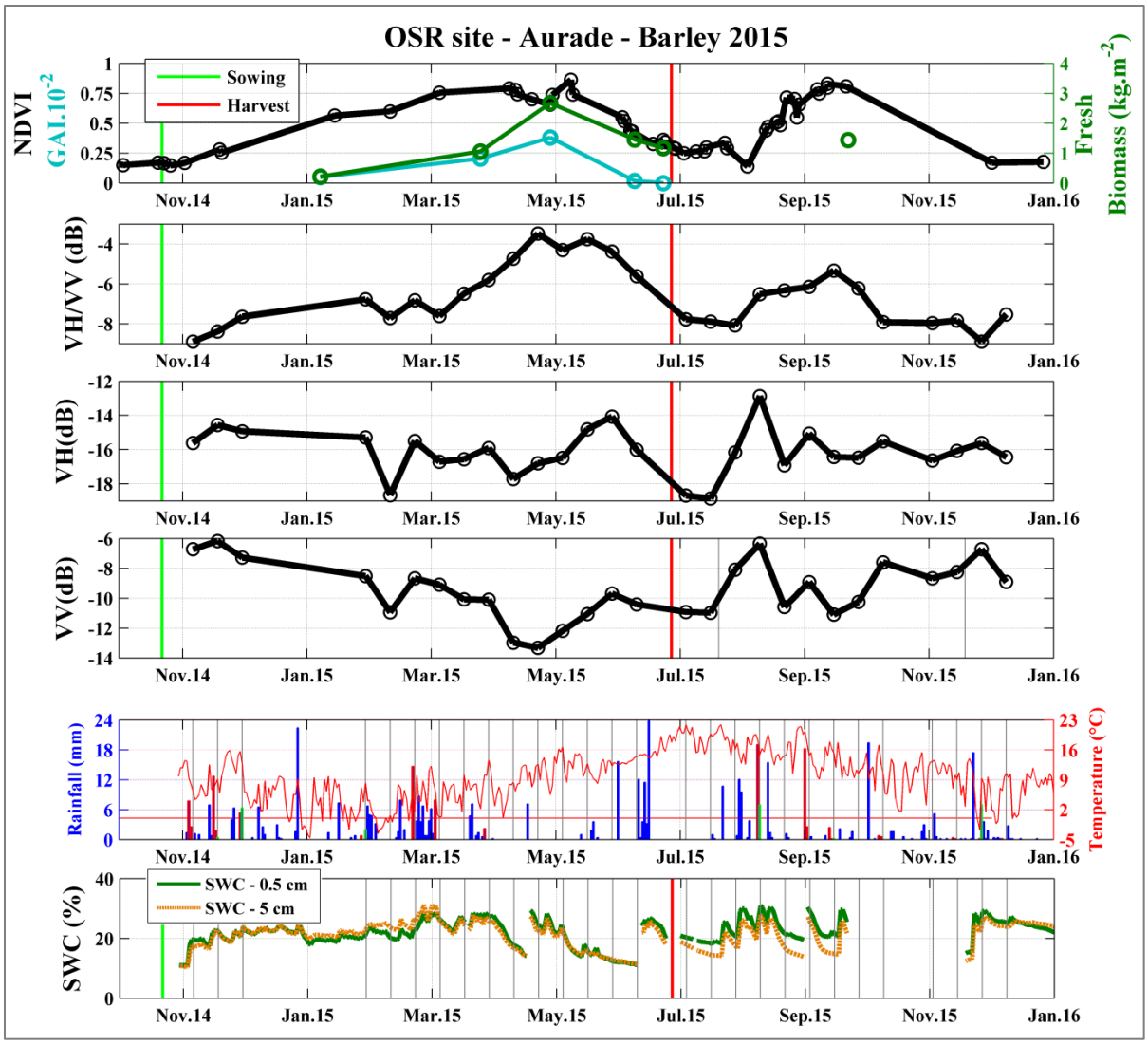

Figure 4: Observations over the barley field: temporal behavior of optical NDVI, radar VH/VV, VH, and VV, rainfalls, temperatures and soil water content (SWC) over the Auradé site, where barley was cultivated in 2015. The blue and green profiles superposed to NDVI are fresh biomass and GAI, respectively. In the second to last plot, temperatures in red were measured at the Sentinel-1 acquisition time 6 a.m. The horizontal red line is the 0°C line. Precipitation is represented by the blue bars. They are displayed in green when occurring in the same days than Sentinel-1 acquisitions and in red if rainfall events take place in the two days before Sentinel-1 acquisitions (assuming that wet soil due to rainfalls may still affect Sentinel-1 backscatter two days later). Vertical grey bars represent Sentinel-1 acquisition events. In the last plot, soil water content (SWC) has been measured at 0.5 cm (green) and 5 cm (brown) depth.

Figure 5 shows the mean values (blue circles) and standard deviations (represented by the filled blue color domains surrounding the mean profile), calculated over the 64 winter wheat fields, as well as the 10 rapeseed fields that will be analysed in the next section. The global behaviors of NDVI, VH/VV, VH and VV over the wheat fields are similar to those of the Auradé barley field from sowing to harvest **(as found by Lopez-Sanchez et al., (2013) at HV polarisation). This finding was expected because the two crops present similar plant structure and functioning, as well as management**

practices. VH/VV and VV are correlated to NDVI (r^2 is 0.74 and 0.58 respectively, *N*=16) contrary to VH (r^2 is approximately 0.01). The decrease of VV at the tillering stage, as explained before, explains this correlation. One interesting feature is that, during this period, the standard deviations of VH and VV between different fields are relatively high (probably revealing the different agricultural practices, but the polarisation ratio VH/VV has a low standard deviation, indicating that the contribution of the ground is reduced in a homogeneous way across all fields.

As demonstrated by the analysis of our available plots, VH/VV is therefore a reliable growth indicator of winter cereals that can be used to separate cereals from other crops such as rapeseed, for example in the frame of a crop type classification, instead of the HH/VV ratio that was found to be reliable as well (Ulaby et al., 1986, Moran et al., 2012, Fieuzal et al., 2013) but not available in the Sentinel-1 IW acquisition mode. Reversely, after harvest, the standard deviations of VH and VV are relatively low, but VH/VV has a high standard deviation, indicating a variety of scattering mechanisms across fields. This is justified by the diversity of post-harvest management practices across the 64 fields, which also explains the lack of a clear second growth cycle (regrowth, cover crop) in the mean optical and radar profiles.

3.1.2. Rapeseed

Compared to the cereal winter crops, rapeseed has earlier sowing/harvest dates and a very different plant structure. At full development, the plants are twice taller (reaching approximately 1.5m), randomly organized with no strong vertical structure.

NDVI and VH/VV (r^2 is 0.30, *N*=16) both follow the vegetation cycle (red profiles in Figure 5), with an earlier start of the NDVI, compared to the cereal winter crops. Also, NDVI reaches high values (above 0.5) shortly after plant emergence, which occurs around October, and remains high until the beginning of senescence in June. On the opposite, VH/VV clearly starts increasing in March, corresponding to the spring growth restart (stem elongation, inflorescence emergence). At the end of flowering and during ripening (end of April-beginning of June), VH/VV remains stable at high values, until it starts decreasing at the beginning of the senescence.

Contrary to the cereal winter crops (displayed in blue in Figure 5), VH and VV follow the VH/VV trend during the growth period, in a similar way although correlation between NDVI and VH (r^2 is 0.38) is greater than with VV (r^2 is 0.25). In fact, taller rapeseed plants compared to cereals, in addition to randomly oriented branches, causes high volume scattering mechanism and lower attenuation of the signal from the ground. **Note that the increasing behavior of VH backscatter for rapeseed during its growth cycle has been previously reported (Yang et al., 2014; Wisemann et al., 2014; Lopez-Sanchez et al., 2013). In particular, in conformity with the results of Wisemann et al. (2014) based**

on RADARSAT-2 data, we observe a small decrease of backscatter at the onset of flowering (beginning of April) and a 5dB increase when the pods reach maturation (May).

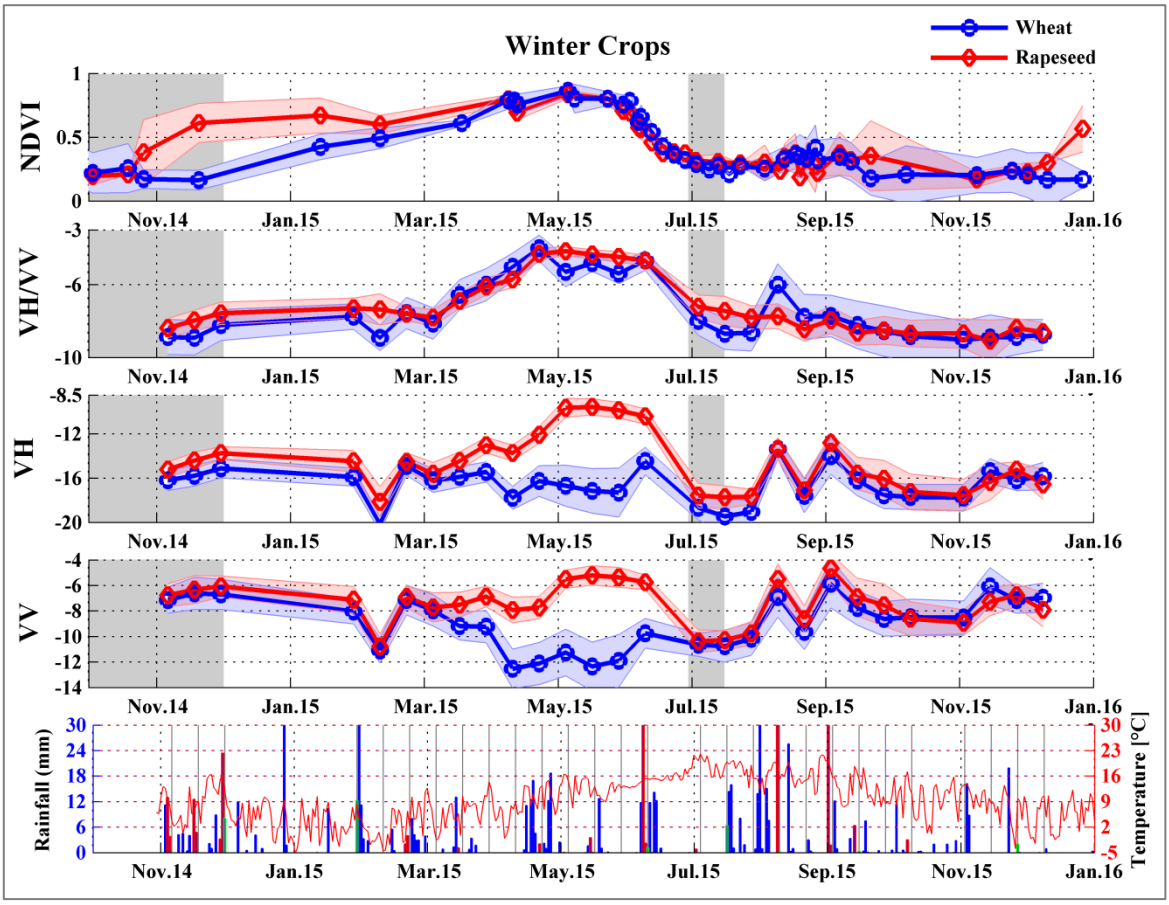

Figure 5: Observations over winter wheat and rapeseed fields: temporal behavior of optical NDVI, radar VH/VV, VH, and VV, rainfalls and temperatures over winter crops, i.e. 64 wheat crops (in blue) and 10 rapeseed crops (in red). Mean values are represented by dots and standard deviations are represented by the filled color domains surrounding the curves. In the last plot (bottom), temperatures in red were measured at the Sentinel-1 acquisition time 6 a.m. Vertical precipitation bars in blue are drawn in green the same days than Sentinel-1 acquisitions and in red the two days before Sentinel-1 acquisitions, assuming that wet soil due to rainfalls may still affect Sentinel-1 backscatter two days later. Vertical grey bars represent Sentinel-1 acquisition events. The typical periods of sowing and harvest are indicated by the grey shaded areas.

3.2. Summer crops

3.2.1. Maize

Maize time series are first analysed in detail for the Lamasquère site (one maize field) with associated *in situ* data in Figure 6 (photographs are shown in Figure S2) and then for a set of summer crop fields (maize, soybean and sunflower) in Figure 7.

In Figure 6, the NDVI and VH/VV ratio are similarly sensitive to the maize phenology. Between the soil work on 26th November and the soil preparation for sowing on 16th April, VH and VV (and VH/VV) steadily decreases due to gradual smoothing of the soil with time (intensified by rainfalls). Just after sowing in the beginning of May, a short decrease of VV and VH (and VH/VV) is observed due to soil work (harrowing) that breaks up, smoothes out and dries the soil surface. Then, the NDVI and VH/VV ratio increase in the same way until the beginning of the harvest on the 8th September. During this period, VH increases because vegetation provides the main volume scattering contribution to the backscattered signal (in fact maize reaches approximately 2.5 m height), and the soil influence becomes marginal (SWC variations shown in Figure 6 do not influence the backscatter).

We can observe that both NDVI and VH/VV profiles are in good agreement with the destructive GAI and fresh biomass measurements. This finding highlights the potential of Sentinel-1 (and Sentinel-2) data for maize biomass retrieval. In the Lamasquère site, there is no senescence stage because maize is harvested when it is still green for silage, which is reflected by an abrupt decrease in NDVI. However, VH/VV decreases gradually from harvest until mid-October. This may be explained by standing green residues (or weed) remaining on the field, which dry out progressively. On 14th October, soil tillage is performed. Soil tillage allows for preparing the soil for the next crop sowing (wheat). This results in the smoothing of the soil surface leading to a decrease in VV, and therefore an increase of VH/VV.

Note that the Lamasquère site was irrigated 5 times between May and August. However, the impact of these irrigation events onto the radar backscatter could not be observed because no Sentinel-1 images were acquired just after irrigation events. In addition, the soil influence becomes very small when maize is well developed. This is the reason why the signal is stable whatever the SWC variations (see Figure 6) as observed in Bériaux et al. (2015) and Fieuzal (2013).

We underline that the results and analysis presented above are based on one single maize field and might be not fully representative of the maize crop behavior, although in line with the results below based on a number of maize fields.

The temporal profiles of the 57 maize fields (in blue), shown together with soybean and sunflower in Figure 7, are similar to the Lamasquère one during the growing period, with correlations r^2 of 0.91 between NDVI and VH/VV and 0.89 between NDVI and VH (N=13). However, trends are not similar during the senescence. Indeed, many fields that are not harvested green for silage show a gradual decrease of NDVI and radar backscatter.

During winter, the soil is bare or the vegetation (such as weeds or re-growth of previous crops) remains short and VV and VH behaviors are mostly due to variations in the soil backscatter.

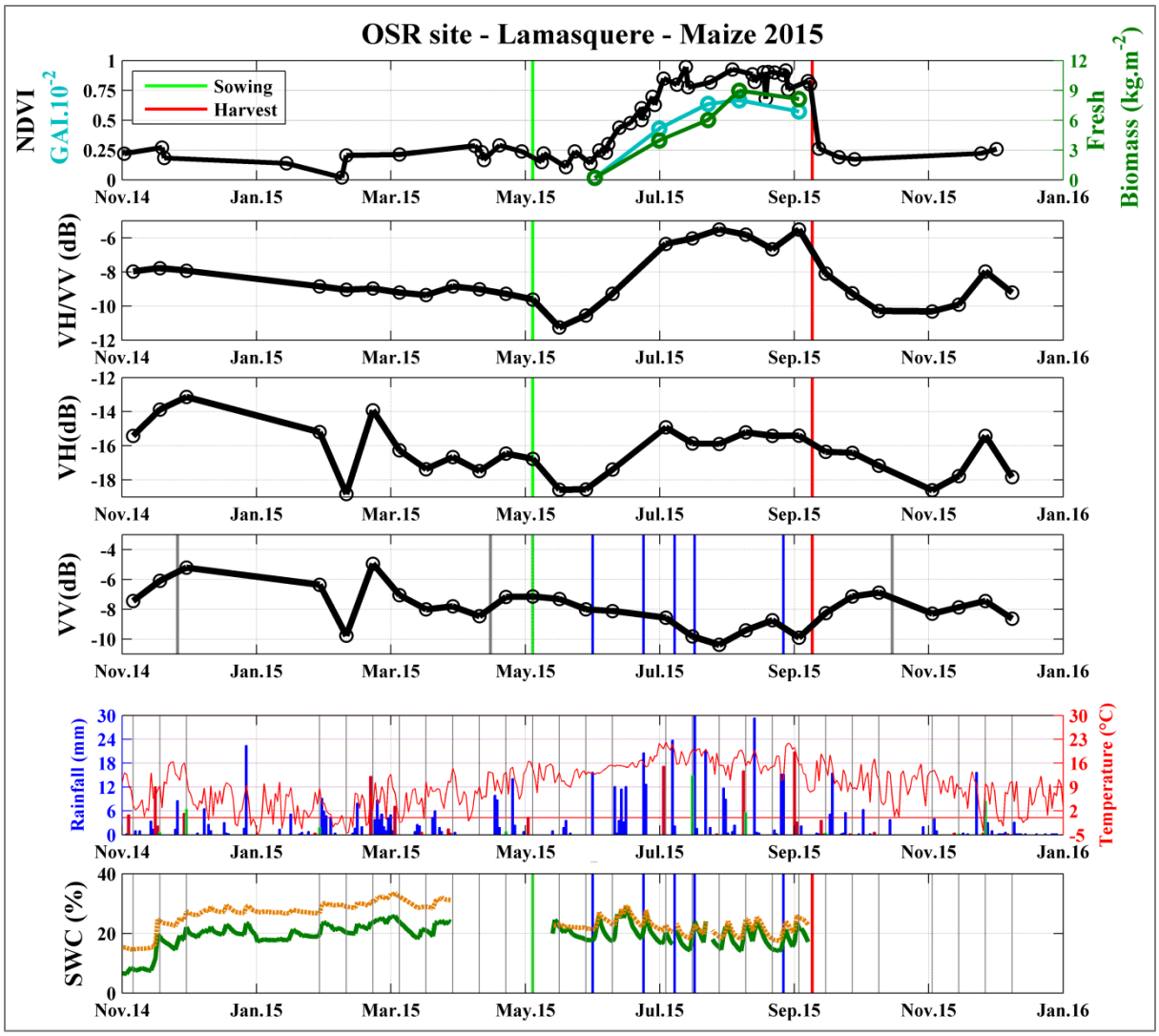

Figure 6: Observations on maize field: temporal behavior of optical NDVI, radar VH/VV, VH, and VV, rainfalls, temperatures and soil water content (SWC) over the Lamasquère site, where maize was cultivated in 2015. The blue and green profiles superposed to NDVI are fresh biomass and GAI, respectively. In the second to last plot, temperatures in red were measured at the Sentinel-1 acquisition time 6 a.m. The horizontal red line is the 0°C line. Precipitation is represented by the blue bars. They are displayed in green when occurring in the same days than Sentinel-1 acquisitions and in red if rainfall events take place in the two days before Sentinel-1 acquisitions (assuming that wet soil due to rainfalls may still affect Sentinel-1 backscatter two days later). Vertical grey bars represent Sentinel-1 acquisition events. In the last plot, SWC has been measured at 0.5 cm (green) and 5 cm (brown) depth. Irrigation events are indicated by the blue bars in the fourth (with VV profile) and in the last plot.

3.2.2. Soybean

The mean and standard deviation time series of 8 soybean crop fields are drawn in green in Figure 7. One can observe very similar NDVI and VH/VV trends (r^2 is 0.82, *N*=13) and both parameters behave almost similarly to maize despite some differences. For example, VV backscatter is lower for soybean than for maize during the growth period. Then, NDVI starts to decrease earlier than VH/VV, despite

VH and VV backscatters start decreasing at the same time as NDVI. Even if the standard deviation at VV polarisation is, as expected, logically higher than for VH when the soil is bare, VH and VV backscatters show similar temporal behaviors, especially during the growing and senescence periods. This may be explained by the fact that the height of soybean only reaches approximately 0.7 m (up to 3 times less than maize) and the number of soybean stems per surface unit is low, which leads to a significant surface scattering from the soil and a poor attenuation of the backscattered signal. In July and August, VV decreases slightly as compared to VH, which explain the lower correlation between NDVI and VV (r^2 is 0.39) than between NDVI and VH (r^2 is 0.69).

3.2.3. Sunflower

Figure 7 shows in red color the temporal behavior of the 116 sunflower fields. The NDVI temporal profile depicts well the growing and senescence period (with a high number of images acquired at that time). Note that NDVI is lower for sunflower than for maize and soybean during the senescence. Likewise, lower GAI were observed for sunflower than for maize (Claverie et al., 2012) and maize and soybean (Claverie, 2012).

VH/VV backscatter is poorly correlated to NDVI (r^2 is 0.08, N=15). Sunflower is therefore the only crop studied in this paper for which temporal monitoring using VH/VV is not recommended. VH backscatter, as for maize and soybean, follows well the NDVI trends (r^2 is 0.71) despite the complex structure of sunflower plants. In addition, sunflower is the only crop for which VV is positively well correlated to NDVI (r^2 is 0.77). In fact, VV is not affected by ground return because of large leaves and both VH and VV are dominated by volume scattering. Therefore, VH/VV does not reduce the surface and double-bounce effect and has smaller sensitivity to volume scattering than for maize and soybean.

At the beginning of July, the flowering stage causes a strong increase of VV that result in a VH/VV decrease, leading to the poor correlation between NDVI and VH/VV.

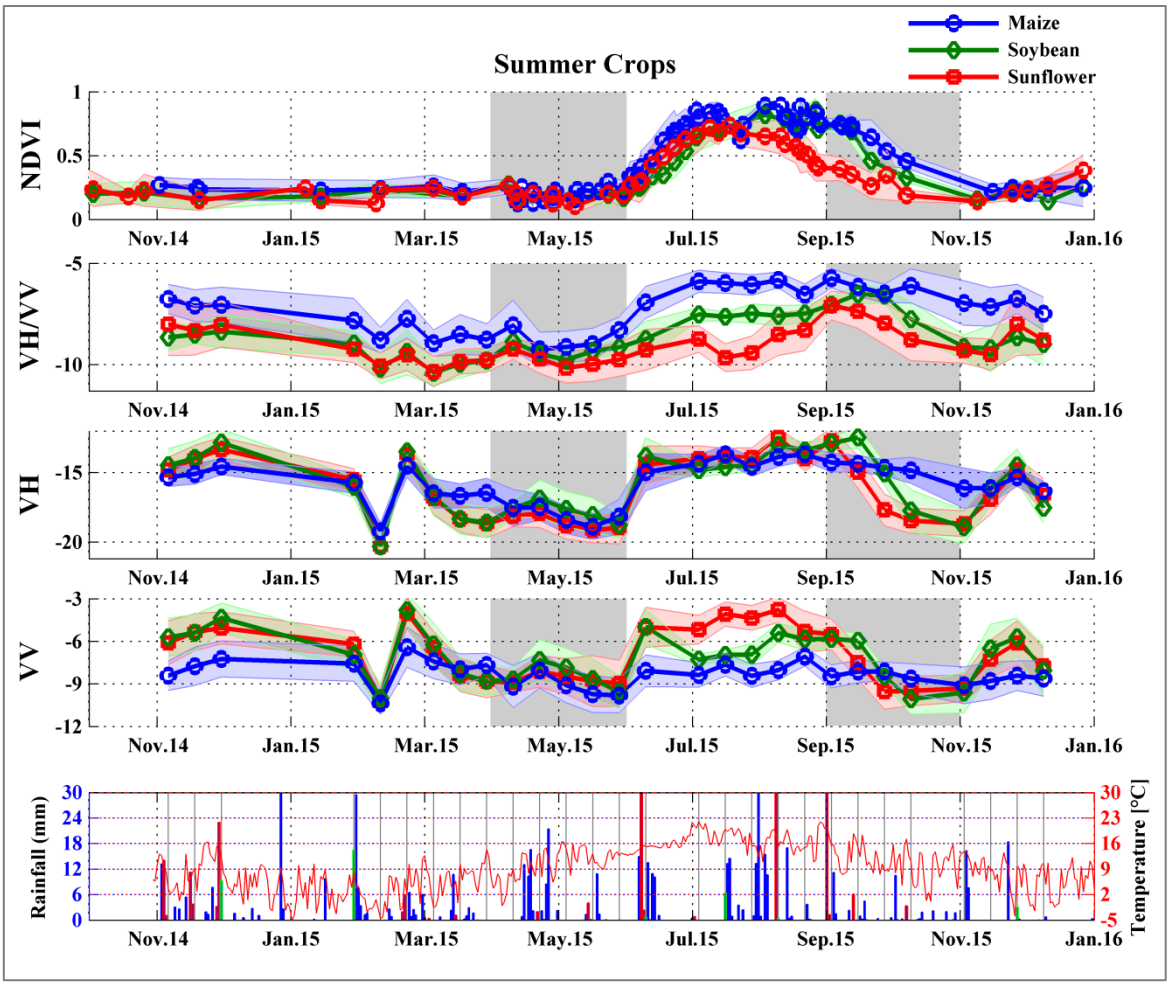

Figure 7: Observations on maize, soybean and sunflower fields: temporal behavior of optical NDVI, radar VH/VV, VH, and VV, rainfalls and temperatures over summer crops, i.e. 57 maize crops (in blue), 8 soybean crops (in green) and 116 sunflower crops (in red). Mean values are represented by dots and standard deviations are represented by the filled color domains surrounding the curves. In the last plot (Bottom), temperatures in red were measured at the Sentinel-1 acquisition time 6 a.m. Vertical precipitation bars in blue are drawn in green the same days than Sentinel-1 acquisitions and in red the two days before Sentinel-1 acquisitions, assuming that wet soil due to rainfalls may still affect Sentinel-1 backscatter two days later. Vertical grey bars represent Sentinel-1 acquisition events. The typical periods of sowing and harvest are indicated by the grey shaded areas.

3.3. Key findings for potential applications

In this section, we summarise some of the main findings of this paper and their potential impact on crop mapping (e.g. crop types, irrigated crops and early crop identification) and biophysical parameters estimation using Sentinel-1 and -2 data.

The analysis and interpretation of Sentinel-1 and Sentinel-2-like time series data led to recommendations for feature selection in the frame of crop mapping. Feature selection is a process by which we look for the best subset of attributes in a dataset. Performing feature selection allows reducing the use of redundant and misleading data to reach highest accuracy, while reducing

computation time. As observed in Figure 5, VH and/or VV SAR backscatters are able to clearly separate winter wheat and rapeseed between the tillering and senescence stages (roughly between March and July). **Satalino et al. (2014) found the same results using the VH backscatter**. In addition, NDVI and VH backscatter may be used to distinguish wheat and rapeseed earlier, i.e. between November and December. Note that VH/VV ratio is less sensitive to cereal development than NDVI before March, suggesting that the use of the VH/VV ratio for winter crop detection may be recommended from March, as found in Inglada et al. (2016). Regarding the classification of summer crops, VH/VV could be used to distinguish maize, soybean and sunflower during the heading/flowering phase (between June and the end of August) as shown in Figure 7, allowing early crop type identification. VV backscatter as well could be used to separate summer crops in July and August. However, using VH is not recommended, except in October for detecting maize crops that are not harvested green for silage. NDVI is not recommended either for distinguishing summer crops, except sunflower during the senescence period, between August and September. This result brings to light the valuable contribution of SAR measurements for distinguishing crop types having similar NDVI profiles.

The analysis and interpretation of Sentinel-1 and Sentinel-2-like time series data also allows enhancing the estimation of the croplands production (biomass and yield) and soil moisture using agro-meteorological models (Revill et al., 2013, Ferrant et al., 2016). **Bernardis et al. (2016) have illustrated this complementarity by using together NDVI (from Landsat), the HH/VV ratio (from TerraSAR-X) air temperatures from a ground-based station for improving rice crop phenological estimation**. In addition, the sensitivity of SAR data to soil moisture may be useful for detecting irrigated crops. This may be useful for crop modeling by providing information on irrigation practices, and also for a better water management strategy.

Our results showed that, for barley and maize crops, the Sentinel-1 and Sentinel-2-like data are correlated to GAI and fresh biomass. Despite the lack of GAI and biomass *in situ* data for rapeseed and soybean, SAR data are likely to be reliable for biomass or GAI estimation given the good agreements between VH/VV and NDVI. GAI time series estimation can be useful for driving crop models, allowing to better set some crop parameters and thus improve the estimation of the model output variables, such as biomass and yield production. Alternatively, SAR data could be used to directly estimate crop biomass, which could be then assimilated by the models, allowing a more accurate estimation of other crop related features, such as the components of carbon fluxes. Besides, during periods of strong cover development, NDVI sensitivity to GAI and biomass is more likely to saturate. Therefore, SAR data could represent a solution for describing crop development under these conditions.

Finally, the joint use of SAR and optical data may allow the development of tillage change maps that are useful in the context of conservative agriculture.

4. Conclusions

In this study, we used a large number of temporal Sentinel-1 together with Sentinel-2-like data to assess the potential of the Sentinel satellites for winter and summer crops monitoring. We applied an adapted multi-image filter to the Sentinel-1 images, taking advantage of the Sentinel-1 dense temporal series to reduce the speckle effect, while preserving the fine structure present in the image, like the crop fields boundaries. The time series of optical NDVI and radar backscatter (VH, VV and VH/VV) were analysed and physically interpreted with the support of rainfall and temperature data, as well as the destructive *in situ* measurements (GAI and fresh biomass, when available). We showed that dense time series allow to capture short phenological stages and thus to precisely describe various crop development.

A better understanding of SAR backscatter and NDVI temporal behaviors under contrasting agricultural practices and environmental conditions will help many upcoming studies related to crop monitoring based on Sentinel-1 and -2, such as dynamic crop mapping and biophysical parameters estimation. Regarding crop mapping, we found that wheat and rapeseed could be better distinguished using VH and VV backscatters between March and July and using NDVI between November and December. Regarding summer crops, we recommend using VH/VV and VV to separate maize, soybean and sunflower during the heading/flowering phase. Results also showed that for barley and maize, both NDVI and VH/VV profiles are in good agreement with the destructive GAI and fresh biomass measurements. Thus, VH/VV ratio could be successfully used for biophysical parameters retrieval and direct biomass assimilation in crop models. VH/VV is also able to detect post-harvest spontaneous regrowth.

In general, SAR and optical data both accurately reproduce crop growth cycles and may be combined for having full gap-free time series, used as inputs for agro-meteorological models. This study points out the interest of SAR data and particularly the VH/VV ratio, which is poorly documented in previous studies (for notable exceptions see McNairn et al., 2009 and Inglada et al., 2016 for crop type classification, Fieuzal et al., 2013 for rapeseed and Blaes et al., 2006 for maize monitoring). Radar data could also be used to fill eventual gaps in the optical data series, namely during cloudy periods. The unprecedented amount of free Sentinel data, guaranteed up to and even beyond 2030 with the next generation of Sentinel, offers a unique opportunity to monitor crops in near real time as highlighted in this study.

5. Acknowledgments

The authors are very grateful to the farmers of Auradé and Lamasquère for granting and facilitating our access to their fields. We also thank the field team (Tiphaine Tallec, Bartosz Zawilski, Aurore Brut, Nicole Ferroni and Hervé Gibrin) for collecting and processing the *in situ* data. Many thanks to Olivier Hagolle for reviewing the optical data section, to Mireille Huc for processing the Deimos data and to Jérôme Cros for help. All optical datasets were processed to level 2A within the THEIA Land Data Center. The authors wish to thank also Silvia Valero for her valuable comments on the paper.

The GSMaP products were distributed by the Earth Observation Research Center, Japan Aerospace Exploration Agency. This work was made possible through the support of the Agence de l'Environnement et de la Maîtrise de l'Energie (ADEME) through the CiCC project, CNRS-INSU that finances the OSR and the Auradé and Lamasquère sites. ICOS-France is also gratefully acknowledged for funding observation data of Lamasquère site. We are thankful to the reviewers for their valuable comments.

References

Aonashi, K., Awaka, J., Hirose, M., Kozu, T., Kubota, T., Liu, G., Shige, S., Kida, S., Seto, S., Takahashi, N., & Takayabu, Y.N. (2009). GSMaP passive, microwave precipitation retrieval algorithm: Algorithm description and validation. J. Meteor. Soc. Japan, 87A, 119-136.

Attema, E. P. W., & Ulaby, F. T. (1978). Vegetation modeled as a water cloud. Radio science, 13(2), 357-364.

Baghdadi, N., Boyer, N., Todoroff, P., El Hajj, M., & Bégué, A. (2009). Potential of SAR sensors TerraSAR-X, ASAR/ENVISAT and PALSAR/ALOS for monitoring sugarcane crops on Reunion Island. Remote Sensing of Environment, 113(8), 1724-1738.

Baret, F., De Solan, B., Lopez-Lozano, R., Ma, K., & Weiss, M. (2010). GAI estimates of row crops from downward looking digital photos taken perpendicular to rows at 57.5 zenith angle: Theoretical considerations based on 3D architecture models and application to wheat crops. Agricultural and Forest Meteorology, 150(11), 1393-1401.

Baret, F., Hagolle, O., Geiger, B., Bicheron, P., Miras, B., Huc, M., ... & Roujean, J. L. (2007). LAI, fAPAR and fCover CYCLOPES global products derived from VEGETATION: Part 1: Principles of the algorithm. Remote sensing of Environment, 110(3), 275-286.

Baup, Frédéric, Rémy Fieuzal, and Julie Betbeder. "Estimation of soybean yield from assimilated optical and radar data into a simplified agrometeorological model." 2015 IEEE International Geoscience and Remote Sensing Symposium (IGARSS). IEEE, 2015.

Bériaux, E., Waldner, F., Collienne, F., Bogaert, P., & Defourny, P. (2015). Maize Leaf Area Index Retrieval from Synthetic Quad Pol SAR Time Series Using the Water Cloud Model. Remote Sensing, 7(12), 16204-16225.

Béziat, P., Ceschia, E., & Dedieu, G. (2009). Carbon balance of a three crop succession over two cropland sites in South West France. Agricultural and Forest Meteorology, 149(10), 1628-1645.

Blaes, X., Defourny, P., Wegmuller, U., Della Vecchia, A., Guerriero, L., & Ferrazzoli, P. (2006). C-band polarimetric indexes for maize monitoring based on a validated radiative transfer model. IEEE transactions on geoscience and remote sensing, 44(4), 791-800.

Bontemps, S., Arias, M., Cara, C., Dedieu, G., Guzzonato, E., Hagolle, O., ... & Rabaute, T. (2015). Building a data set over 12 globally distributed sites to support the development of agriculture monitoring applications with Sentinel-2. Remote Sensing, 7(12), 16062-16090.

Bouman, B. A., & Hoekman, D. H. (1993). Multi-temporal, multi-frequency radar measurements of agricultural crops during the Agriscatt-88 campaign in The Netherlands. Remote Sensing, 14(8), 1595-1614.

Brown, S. C. M., Cookmartin, G., Morrison, K., McDonald, A. J., Quegan, S., Anderson, C., ... & Dampney, P. (2000). Wheat scattering mechanisms observed in near-field radar imagery compared with results from a radiative transfer model. In Geoscience and Remote Sensing Symposium, 2000. Proceedings. IGARSS 2000. IEEE 2000 International (Vol. 7, pp. 2933-2935). IEEE.

Brown, S. C., Quegan, S., Morrison, K., Bennett, J. C., & Cookmartin, G. (2003). High-resolution measurements of scattering in wheat canopies-Implications for crop parameter retrieval. IEEE Transactions on Geoscience and Remote Sensing, 41(7), 1602-1610.

Bruniquel, J., & Lopes, A. (1997). Multi-variate optimal speckle reduction in SAR imagery. International journal of remote sensing, 18(3), 603-627.

Bush, T. F. (1976). Monitoring wheat growth with radar.

Ceschia, Eric, et al (2010). "Management effects on net ecosystem carbon and GHG budgets at European crop sites." Agriculture, Ecosystems & Environment, 139.3: 363-383.

Chiu, T., & Sarabandi, K. (2000). Electromagnetic scattering from short branching vegetation. IEEE Transactions on Geoscience and Remote Sensing, 38(2), 911-925.

Claverie, M., Demarez, V., Duchemin, B., Hagolle, O., Ducrot, D., Marais-Sicre, C., ... & Fieuzal, R. (2012). Maize and sunflower biomass estimation in southwest France using high spatial and temporal resolution remote sensing data. Remote Sensing of Environment, 124, 844-857.

Claverie, M. (2012). Estimation spatialisée de la biomasse et des besoins en eau des cultures à l'aide de données satellitales à hautes résolutions spatiale et temporelle: application aux agrosystèmes du sud-ouest de la France (Doctoral dissertation, Université de Toulouse, Université Toulouse III-Paul Sabatier).

Cookmartin, G., Saich, P., Quegan, S., Cordey, R., Burgess-Allen, P., & Sowter, A. (2000). Modeling microwave interactions with crops and comparison with ERS-2 SAR observations. IEEE Transactions on Geoscience and Remote Sensing, 38(2), 658-670.

Deschamps, B., McNairn, H., Shang, J., & Jiao, X. (2012). Towards operational radar-only crop type classification: comparison of a traditional decision tree with a random forest classifier. Canadian Journal of Remote Sensing, 38(1), 60-68.

Dobson, M. C., Pierce, L. E., & Ulaby, F. T. (1996). Knowledge-based land-cover classification using ERS-1/JERS-1 SAR composites. IEEE Transactions on Geoscience and Remote Sensing, 34(1), 83-99.

Doraiswamy, P. C., Hatfield, J. L., Jackson, T. J., Akhmedov, B., Prueger, J., & Stern, A. (2004). Crop condition and yield simulations using Landsat and MODIS. Remote sensing of environment, 92(4), 548-559.

Duchemin, B., Fieuzal, R., Rivera, M. A., Ezzahar, J., Jarlan, L., Rodriguez, J. C., ... & Watts, C. (2015). Impact of sowing date on yield and water use efficiency of wheat analyzed through spatial modeling and FORMOSAT-2 images. Remote Sensing, 7(5), 5951-5979.

Duveiller, G., Weiss, M., Baret, F., & Defourny, P. (2011). Retrieving wheat Green Area Index during the growing season from optical time series measurements based on neural network radiative transfer inversion. Remote Sensing of Environment, 115(3), 887-896.

Engdahl, M. E., Borgeaud, M., & Rast, M. (2001). The use of ERS-1/2 tandem interferometric coherence in the estimation of agricultural crop heights. IEEE transactions on geoscience and remote sensing, 39(8), 1799-1806.

ESA, 2017. The Sentinel Application Platform **(SNAP), a common architecture for all Sentinel Toolboxes being jointly developed by Brockmann Consult, Array Systems Computing and C-S. Downloadable on *http://step.esa.int/main/download/*. European Space Agency (ESA).**

ESA Report 2016. Sentinel-1 product definition. *https://sentinel.esa.int/documents/247904/1877131/Sentinel-1-Product-Definition* Accessed 23 April 2016.

Ferrant, S., Gascoin, S., Veloso, A., Salmon-Monviola, J., Claverie, M., Rivalland, V., ... & Durand, P. (2014). Agro-hydrology and multi temporal high resolution remote sensing: toward an explicit spatial processes calibration. Hydrology and Earth System Sciences Discussions (HESSD), 11(7), 7689-7732.

Ferrant, S., Bustillo, V., Burel, E., Salmon-Monviola, J., Claverie, M., Jarosz, N., ... & Ceschia, E. (2016). Extracting Soil Water Holding Capacity Parameters of a Distributed Agro-Hydrological Model from High Resolution Optical Satellite Observations Series. Remote Sensing, 8(2), 154.

Fieuzal, R., Baup, F., & Marais-Sicre, C. (2013). Monitoring wheat and rapeseed by using synchronous optical and radar satellite data—From temporal signatures to crop parameters estimation.

Fieuzal, R. (2013). Apports de données radar pour l'estimation des paramètres biophysiques des surfaces agricoles (Doctoral dissertation, Université de Toulouse, Université Toulouse III-Paul Sabatier).

Fieuzal, R., and F. Baup. "Estimation of leaf area index and crop height of sunflowers using multi-temporal optical and SAR satellite data." International Journal of Remote Sensing (2016): 1-30.

Hagolle, O.; Dedieu, G.; Mougenot, B.; Debaecker, V.; Duchemin, B.; Meygret, A. Correction of aerosol effects on multi-temporal images acquired with constant viewing angles: Application to Formosat-2 images. Remote Sens. Environ. 2008, 112, 1689–1701.

Hagolle, O.; Sylvander, S.; Huc, M.; Claverie, M.; Clesse, D.; Dechoz, C.; Lonjou, V.; Poulain, V. SPOT4 (Take5): Simulation of Sentinel-2 Time Series on 45 Large sites. Remote Sens. 2015, 7, 12242–12264.

Hagolle, O.; Huc, M.; Villa Pascual, D.; Dedieu, G. A multi-temporal and multi-spectral method to estimate aerosol optical thickness over land, for the atmospheric correction of FormoSat-2, LandSat, VENuS and Sentinel-2 images. Remote Sens. 2015, 7, 2668–2691.

Hagolle, O.; Huc, M.; Villa Pascual, D.; Dedieu, G. A multi-temporal method for cloud detection, applied to Formosat-2, VENuS, Landsat and Sentinel-2 images. Remote Sens. Environ. 2010, 114, 1747–1755.

Hajnsek, I., Horn, R., Scheiber, R., Bianchi, R., Davidson, M. (2007): The AGRISAR Campaign: Monitoring the Vegetation Cycle using Polarimetric SAR Data. In: H. Lacoste & L. Ouwehand (Eds.) ESA Conference Proceedings SP-636: EnviSat Symposium 2007 (CD).

Inglada, J., Arias, M., Tardy, B., Hagolle, O., Valero, S., Morin, D., ... & Koetz, B. (2015). Assessment of an operational system for crop type map production using high temporal and spatial resolution satellite optical imagery. Remote Sensing, 7(9), 12356-12379.

Inglada, J., Vincent, A., Arias, M., & Marais-Sicre, C. (2016). Improved Early Crop Type Identification By Joint Use of High Temporal Resolution SAR And Optical Image Time Series. Remote Sens., 8(5), 362.

Jia, M., Tong, L., Zhang, Y., & Chen, Y. (2013). Multitemporal radar backscattering measurement of wheat fields using multifrequency (L, S, C, and X) and full-polarization. Radio Science, 48(5), 471-481.

Karam, M. A., Fung, A. K., Lang, R. H., & Chauhan, N. S. (1992). A microwave scattering model for layered vegetation. IEEE Transactions on Geoscience and Remote Sensing, 30(4), 767-784.

Khaldoune, J., Van Bochove, E., Bernier, M., & Nolin, M. C. (2011). Mapping agricultural frozen soil on the watershed scale using remote sensing data. Applied and Environmental Soil Science, 2011.

Le Page, M., Toumi, J., Khabba, S., Hagolle, O., Tavernier, A., Kharrou, M. H., ... & Yousfi, M. (2014). A life-size and near real-time test of irrigation scheduling with a Sentinel-2 Like Time Series (SPOT4-Take5) in Morocco. Remote Sensing, 6(11), 11182-11203.

Lopez-Sanchez, J. M., Vicente-Guijalba, F., Ballester-Berman, J. D., & Cloude, S. R. (2013, September). Estimating phenology of agricultural crops from space. In ESA Living Planet Symp., Edinburgh, UK.

Mattia, F., Le Toan, T., Picard, G., Posa, F. I., D'Alessio, A., Notarnicola, C., ... & Pasquariello, G. (2003). Multitemporal C-band radar measurements on wheat fields. IEEE Transactions on Geoscience and Remote Sensing, 41(7), 1551-1560.

Mattia, F., Satalino, G., Dente, L., & Pasquariello, G. (2006). Using a priori information to improve soil moisture retrieval from ENVISAT ASAR AP data in semiarid regions. IEEE transactions on geoscience and remote sensing, 44(4), 900-912.

McNairn, H., & Brisco, B. (2004). The application of C-band polarimetric SAR for agriculture: a review. Canadian Journal of Remote Sensing, 30(3), 525-542.

McNairn, H., Champagne, C., Shang, J., Holmstrom, D., & Reichert, G. (2009). Integration of optical and Synthetic Aperture Radar (SAR) imagery for delivering operational annual crop inventories. ISPRS Journal of Photogrammetry and Remote Sensing, 64(5), 434-449.

McNairn, H., Kross, A., Lapen, D., Caves, R., & Shang, J. (2014). Early season monitoring of corn and soybeans with TerraSAR-X and RADARSAT-2. International Journal of Applied Earth Observation and Geoinformation, 28, 252-259.

Mermoz, S., Le Toan, T., Villard, L., Réjou-Méchain, M., & Seifert-Granzin, J. (2014). Biomass assessment in the Cameroon savanna using ALOS PALSAR data. Remote Sensing of Environment, 155, 109-119.

Mermoz, S., & Le Toan, T. (2016). Forest disturbances and regrowth assessment using ALOS PALSAR data from 2007 to 2010 in Vietnam, Cambodia and Lao PDR. Remote Sensing, 8(3), 217.

Moran, M. S., Alonso, L., Moreno, J. F., Mateo, M. P. C., De La Cruz, D. F., & Montoro, A. (2012). A RADARSAT-2 quad-polarized time series for monitoring crop and soil conditions in Barrax, Spain. IEEE Transactions on Geoscience and Remote Sensing, 50(4), 1057-1070.

Navarro, A., Rolim, J., Miguel, I., Catalão, J., Silva, J., Painho, M., & Vekerdy, Z. (2016). Crop Monitoring Based on SPOT-5 Take-5 and Sentinel-1A Data for the Estimation of Crop Water Requirements. Remote Sensing, 8(6), 525.

Picard, G., & Toan, T. L. (2002). A multiple scattering model for C-band backscatter of wheat canopies. Journal of Electromagnetic Waves and Applications, 16(10), 1447-1466.

Picard, G., Le Toan, T., & Mattia, F. (2003). Understanding C-band radar backscatter from wheat canopy using a multiple-scattering coherent model. IEEE Transactions on Geoscience and Remote Sensing, 41(7), 1583-1591.

Poeplau, Christopher, and Axel Don 2015. "Carbon sequestration in agricultural soils via cultivation of cover crops–A meta-analysis." Agriculture, Ecosystems & Environment, 200: 33-41.

Quarmby, N. A., Milnes, M., Hindle, T. L., & Silleos, N. (1993). The use of multi-temporal NDVI measurements from AVHRR data for crop yield estimation and prediction. International Journal of Remote Sensing, 14(2), 199-210.

Quegan, S., & Yu, J. J. (2001). Filtering of multichannel SAR images. *Geoscience and Remote Sensing, IEEE Transactions on*, *39*(11), 2373-2379.

Revill, A., Sus, O., Barrett, B., & Williams, M. (2013). Carbon cycling of European croplands: A framework for the assimilation of optical and microwave Earth observation data. Remote Sensing of Environment, 137, 84-93.

Schmugge, T. J. (1983). Remote sensing of soil moisture: Recent advances. IEEE Transactions on Geoscience and Remote Sensing, (3), 336-344.

Skriver, H., Mattia, F., Satalino, G., Balenzano, A., Pauwels, V. R., Verhoest, N. E., & Davidson, M. (2011). Crop classification using short-revisit multitemporal SAR data. IEEE Journal of Selected Topics in Applied Earth Observations and Remote Sensing, 4(2), 423-431.

Steele-Dunne, S. C., McNairn, H., Monsivais-Huertero, A., Judge, J., Liu, P. W., & Papathanassiou, K. (2017). Radar Remote Sensing of Agricultural Canopies: A Review. IEEE Journal of Selected Topics in Applied Earth Observations and Remote Sensing.

Ulaby, F. T., Moore, R. K., & Fung, A. K. (1986). Microwave remote sensing active and passive-volume III: from theory to applications.

Veloso, A. (2014). Regional estimates of the production, fluxes and budgets of carbon and water for winter wheat by using high resolution remote sensing data combined with a crop model: Application to southwest France. Doctoral dissertation. Université Toulouse III- Paul Sabatier, Toulouse, France. ***http://www.cesbio.ups-tlse.fr/data_all/theses/Th_Veloso_2014.pdf***

Wiseman, G., McNairn, H., Homayouni, S., & Shang, J. (2014). RADARSAT-2 polarimetric SAR response to crop biomass for agricultural production monitoring. IEEE Journal of Selected Topics in Applied Earth Observations and Remote Sensing, 7(11), 4461-4471.

Yang, H., Li, Z., Chen, E., Zhao, C., Yang, G., Casa, R., ... & Feng, Q. (2014). Temporal polarimetric behavior of oilseed rape (Brassica napus L.) at C-band for early season sowing date monitoring. Remote Sensing, 6(11), 10375-10394.